NONDESTRUCTIVE TESTING AND EVALUATION
https://doi.org/10.1080/10589759.2024.2402885

Taylor & Francis
Taylor & Francis Group

New evaluation method for defects propagation in toroidal roller bearings using dominant frequency of acoustic emission

Housam Mohammad [a], Frantisek Vlasic [a], Baraah Maya [b], Mhd.Ali Shehadeh [c] and Pavel Mazal [a]

[a]Institute of Machine and Industrial Design, Brno University of Technology, Brno, Czechia; [b]Institute of mathematics, Brno University of Technology, Brno, Czechia; [c]Institute of Automation, Brno University of Technology, Brno, Czechia

ABSTRACT

The increased use of roller bearings in recent years has made it vital to develop techniques for Condition Monitoring (CM) of these valuable assets. Toroidal Roller Bearings (TRB) are one of the recent inventions that has revolutionised some industries because of its unique design. In this study, newly produced TRBs were tested using Acoustic Emission (AE), vibration and temperature, on a specially designed test rig. The AE signal was recorded, processed, and analysed using FFT-based methods to transform from the time domain to the frequency domain, and to specify the Dominant Frequency (DF) of each hit in the signal. The result of the analysis was a layout on the time domain of the DFs of all AE hits along with RMS_{AE} and other parameters, this layout was called DF map. The test was divided into three phases, and the DF bands were divided horizontally into three band groups. The aim is to establish a correlation between the phases and DF bands. Knowing the type of defects that are typical for each phase in the test provided insights to what are the DFs of that type. Promising results can be achieved using this measuring method on other types of bearings.

ARTICLE HISTORY
Received 15 July 2024
Accepted 5 September 2024

KEYWORDS
Acoustic emission; toroidal roller bearings; dominant frequency; frequency domain; condition monitoring

Introduction

In recent decades, the field of non-destructive testing (NDT) has witnessed the emergence of various techniques designed to diagnose defects in materials or structures without compromising their integrity. Among these, the Acoustic Emission (AE) technique has gained significant attention due to its unique capability to dynamically track the entire damage process of materials with minimal constraints on the operational conditions, environmental factors, and failure mechanisms [1]. AE involves the generation of transient elastic waves resulting from the sudden release of strain energy, such as that from deformation or fracture, within a stressed material or structure [2–5]. Acoustic Emission (AE) is defined as the class of phenomena whereby

CONTACT Housam Mohammad Housam.mohammad@vutbr.cz

transient elastic waves are generated by the rapid release of energy from localised sources within a material [6–8]. The AE is accompanied by the emission of elastic stress waves that occur over a wide frequency range but typically from 100 kHz to 1 MHz [9]. The AE technique is considered one of the most accurate monitoring methods in machining that some researchers used it to identify damage mechanisms [9]. AE waves contain valuable information related to the microstructural changes in the material and therefore can be used to detect structural defects without any external ultrasonic inputs [10]. Because of its high sensitivity and great potentials, AE has been increasingly used in the field of CM of bearings. The advancements in its frequency-domain properties and parameters made it even more attractive, which is one of the reason we adopted this method in our current study, and we applied it on a relatively new type of bearing.

A distinctive characteristic of the AE technique sets it apart from other NDT methods is that rather than emitting signals towards the object under investigation, AE sensors receive transient elastic waves released from localised sources within the test object due to the transient relaxation of stress and strain fields [11]. When an AE sensor (transducer) is affixed to a structure undergoing dynamic changes, it detects a portion of the energy released in the form of elastic waves, which, if interpreted correctly, can specify the nature of structural changes taking place. Notably, it is highly sensitive in detecting defect initiation and propagation stages [12].

AE technique has been proven to also have the capacity for subsurface fault detection of roller bearings. As shown in a recent study by Hidle, E. et al. [13], where in a laboratory durability test of a roller bearing element, initiated roller contact fatigue damage under controlled conditions, and the accompanying AE waveforms were acquired and analysed. Their proposed method combined information theory and autoencoder to achieve high sensitivity in AE signals. Using a probabilistic framework presented in [14] R. Fuentes et al. were able to arrive at a similar conclusion.

Regarding the use of AE frequency parameters, XU, Peifei et al. [15] suggested the use of parameters peak frequency and peak amplitude to classify the damage modes, because their different ranges represent different damage modes that could be clustered robustly. According to the authors, the largest variance percentage is the peak frequency reaching 0.5, and it is far larger than the second feature average frequency. Therefore, the peak frequency of AE signals is the best feature selected to identify the damage modes due to the high discrete degree of AE signals.

The importance of the time-frequency features of AE signal was evident in the work of Yu, Yang, et al. [16] when they used the time-frequency coherence (TFC) and time-frequency energy change rate of AE for fault diagnosis on cylindrical roller bearings. They analysed other time-frequency methods and showed that their TFC is more resistant to interference. Another recent work that showed the importance of the analyses on the frequency domain of AE was carried out by Jiangbo, C. et al. [17], where they used the wavelet packet decomposition to transform the AE signal to the frequency domain and correlate the resulting frequency bands with failure modes of the specimen.

Poddar and Tandon [18] concluded from their measurements on journal bearings using AE and Vibration that AE activities resulting from asperity interaction have significant energy in the frequency range of 100–400 kHz with peak frequencies in the range of 224–283 kHz, and the peak frequency shifts from the higher to

the lower side as the asperity interaction transits from the elastic to plastic contact. This correspondence derived from the spectral analysis of AE signals could be very useful in developing CM parameters to proactively prevent bearing failure.

With regard to the use of frequency domain parameters of AE signal in CM of materials, a comprehensive look at the current state of knowledge shows that it has been rapidly developing recently, since it has been proven that these parameters provide insights into the signal that cannot be seen otherwise. Some of the basic frequency parameters include the dominant frequency (sometimes called the peak frequency), initiation frequency, average frequency, reverberating frequency, and the frequency centroid [19]. A more thorough investigation in the literature shows that the dominant frequency has been used much more often than the other frequency parameters. The DF of AE signal is defined as the frequency corresponding to the highest point of amplitude in the 2D spectrogram [20]. As presented by many studies, DF is a leading indicator for explaining the spectrum characteristics of AE signals [12,20], and its characteristics provide significant controls on investigations of microscopic fractures [21]. Recently, Dong, L. et al. [22] stated that the DF is the main carrier of the energy of the AE source, whereas the DF of AE in the rock failure test is concentrated in specific frequency bands. In a study on damage evolution of welding defects using AE by Zhou Wei, et al. [23], peak frequency of AE was proved to be a decisive factor in determining the welding defect.

Many other studies in the field of geotechnical engineering have used frequency parameters of AE, including DF, as explored by [21,24–27], and [28] where they all use similar techniques regarding the extraction and analysis methods of those parameters. On the other hand, in the area of defect detection and CM of rolling bearings, despite the extensive use of AE and the advancement of research works, the frequency parameters of AE hits have not been taken much into consideration.

To address this research gap, this study concentrates on the use of the main frequency domain parameter, which is the DF of AE hits, as the main determinant for the condition of the monitored object. Therefore, it introduces a new method for the evaluation and CM of roller bearings based on the use of DF of AE hits as a parameter that corresponds to the type of defect that produces those AE hits. Toroidal roller bearings were used as specimens in the experiments, but the results of this method could be extended to other types of roller bearings. Along with AE as a tool for damage detection, vibration and temperature were used for the purpose of comparison and confirmation of the results.

The remainder of this paper is organised as follows: the second section (Methods) describes the specimen properties, equipment, measurement setup, and data acquisition procedure; the third section (Results) describes and explains the vibration and AE analyses and outlines the results of the measurements; the fourth section (Discussion) analyzes the meaning of the results and puts them into perspective; and the fifth section (Conclusion) summarises the main results in a brief manner and introduces a glimpse into the following steps.

Methods

The experiment setup

The measurements were performed in the laboratories of the bearing company ZKL, which is one of the biggest producers of bearings in the middle of Europe. The test rig that has been used in the experiments was designed and constructed for this type of measurement. This test rig consists of a special split housing that contains a core part. The core part, shown below in Figure 1, consists of a shaft and three adaptable sleeves that enclose three bearings, those are: the two support bearings (cylindrical) on the edges and one tested toroidal roller bearing (TRB) in the middle.

The reason for choosing TRB as a test specimen is that it is one of the emerging types of roller bearings that has been gaining considerable attention in the industry since its introduction by SKF under their trademark CARB®. After the expiration of the patent for SKF many other companies followed the production and investment in this type of bearing, which has unique features that no other bearing alone can provide. Other variations of this bearing were introduced by other producers (such as ADAPT from Timken and TORB from Schaeffler), but with the same principle. Simply put, TRB is a single row, compact self-aligning bearing with long, crowned rollers [29]. The concave raceways in the inner and outer rings are part of a toroid, ideally are part of the same toroid. These raceway profiles ensure optimum distribution of stresses in the bearing as well as low operating friction, as can be seen in Figure 2. The toroidal profile allows self-

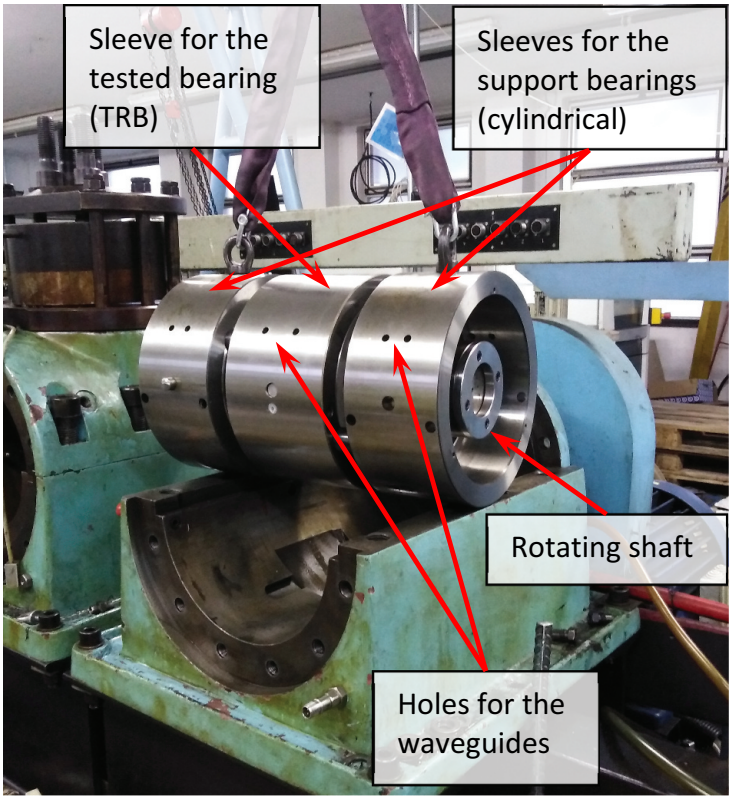

Figure 1. The core part of the housing which contains the two support bearings and one tested bearing.

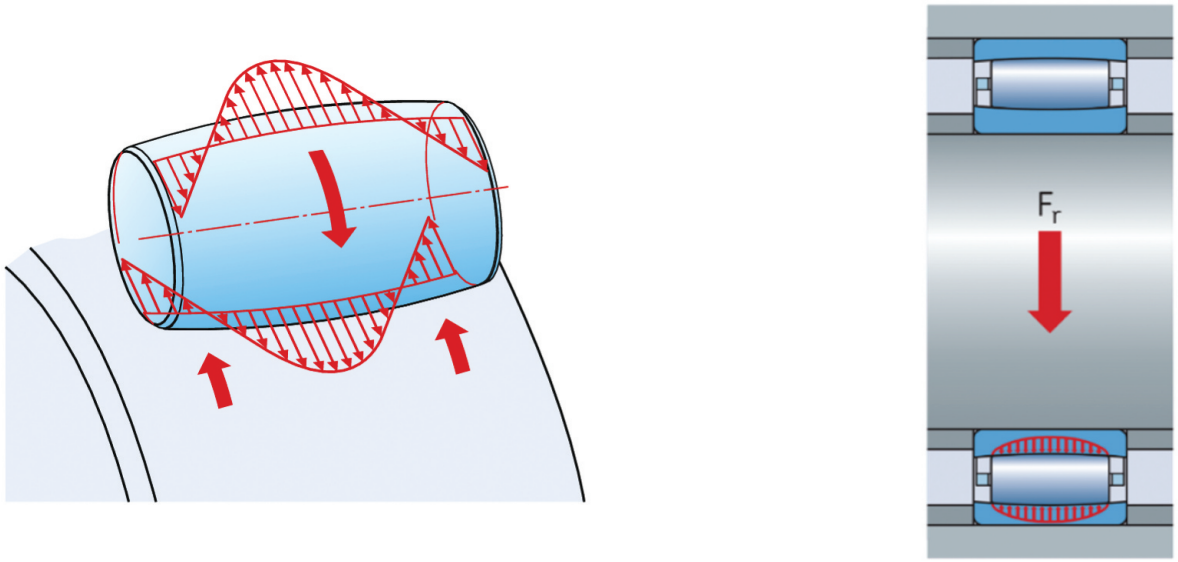

Figure 2. The distribution of force on the self-aligning, low friction bearing (with permission to publish from skf.Cz).

guiding for the rollers inside the raceways, which means they will always adapt to the position at which the load is distributed over the length of the roller [30].

TRBs have been investigated in research where they were used as specimens of roller bearings, such as the work of Benchea M. et al. [31] when they studied the influence of surface roughness on active surfaces geometry and on modified rating life of rolling contacts, and the work of Fritzson D. et al. [32] in their computational simulation of the rolling bearings. Despite the importance of TRBs, not many research work was done on them, the high price of those bearings could be one reason for that. However, big players in the bearing industry have been doing their own research, not a scientifically reviewed research but an industry-oriented one, on the properties and improvements in TRBs, such as [33] by SKF group about the axial displacement verifications and other design considerations, and [34] by Schaeffler tech. about geometrical restrictions and reduction of internal radial clearance in TRBs.

In this study, the tested TRB was of the type C4026V. We tested five identical recently-produced bearings in these experiments, where each test lasted for 3–6 days. The material of all bearing parts is high-carbon chromium bearing steel GCr15SiMn, which is hardened and tempered to hardness HRC 58 for the rings and HRC 61 for the rollers. It is a full complement bearing (without a cage) to increase its load rating, but this decreases its speed rating. Basic geometrical specifications of the tested toroidal bearing are listed in Table 1.

The split housing that contains the core part is general-purpose housing made of cast iron. A hydraulic loading system is mounted on this housing as shown in Figure 3., it is controlled by a PLC driving system, which allows controllable loading during the test. The loading on the bearing during these tests was chosen to be 3 MPa, and the rotation speed of the shaft was set at 500 r.p.m. These values were selected based on previous tests and comparisons with the same type of bearing. The tested bearing was submerged in oil bath, where the oil level was guaranteed to remain above the lowest rolling element as specified by the design standard of this testing stand. The oil bath guarantees continuous

Table 1. Geometrical properties of the tested toroidal bearing.

Property	Value
Outer diameter (D)	200 mm
Bore diameter (d)	130 mm
Width	69 mm
Radial internal clearance	150 µm
Basic static load rating	1120 kN
Basic dynamic load rating	720 kN
Cage	Without
Locating feature	Without

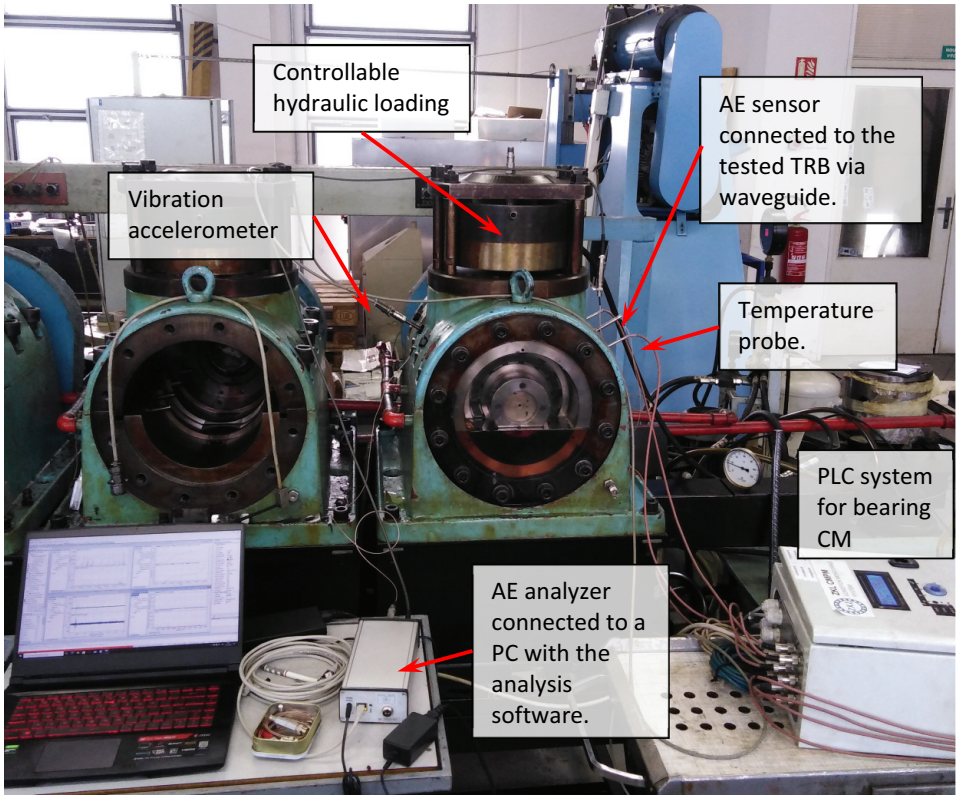

Figure 3. The experiment setup.

lubrication of the whole testing space, it is more suitable for high rotation speeds, better in dissipating temperature and in flushing away all kinds of contaminants, and it is best suited for our unsealed specimens of TRBs.

The upper part of the split housing contains channels drilled to accommodate the waveguides, which transmit the AE and vibration signals to the AE sensor and the vibration transducer (accelerometer), respectively. Temperature probes are also inserted through specific holes to measure the temperature of the outer rings, and the oil temperature. The AE waveguide is ensured to be fixed in constant contact with the outer ring of tested bearing, and it is fixed as close as possible to the load, so that it can receive the signals from the loaded zone of the tested bearing. The AE sensors (from the type ZD Rpety – DAKEL) are firmly attached to those waveguides, as shown in the schematic drawing in Figure 4. Two AE sensors were used in the experiments: one (sensor A) was attached to a waveguide, and the second (sensor B) was attached to the

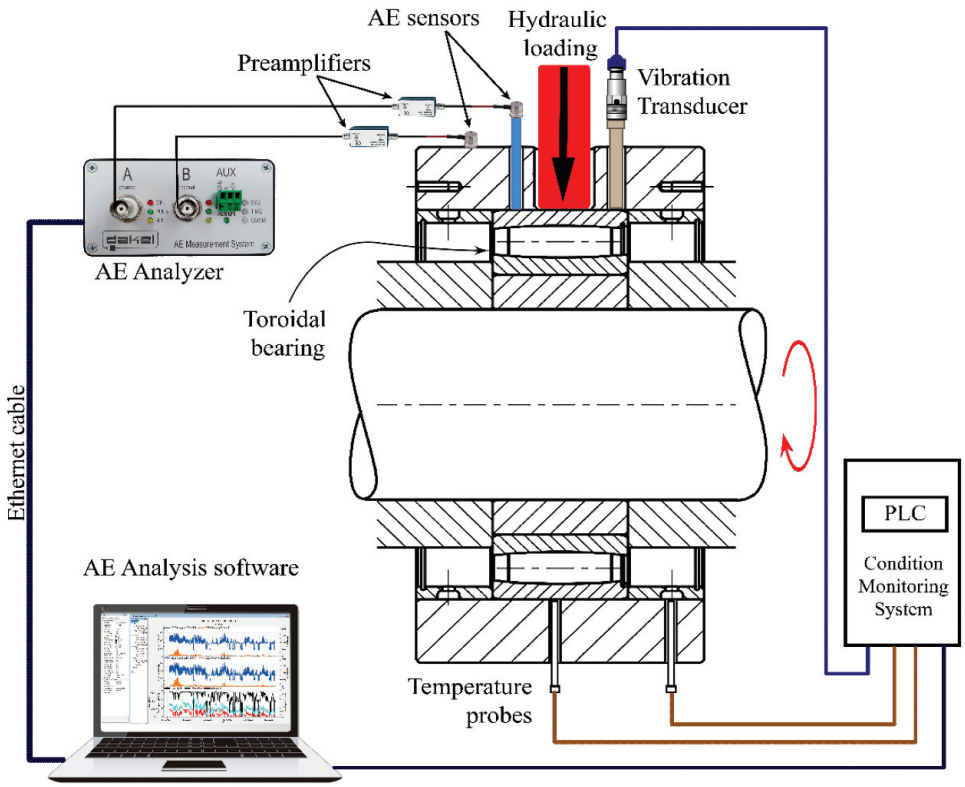

Figure 4. Schematic drawing of the experiment.

housing of the bearings and the signal it received was used just as a reference. The type of AE sensor used in this experiment is MDK-13, which has a built-in magnet to improve the stability of the sensor on ferromagnetic surfaces. We added a preamplifier with a gain around 20 dB to each AE sensor. The frequency range for best sensitivity is [20–400 kHz]. The AE analyser is Dakel-ZEDO-22, with two channels, which is connected to the software Zdaemon installed on a PC, which is also connected to the PLC system responsible for controlling the entire measurement. The vibration transducer and the temperature probes were connected to the PLC monitoring system. The sampling frequency for vibration readings is 10 Hz, and for Temperature is 1 Hz. The sampling frequency for AE signal measurement was set to 5 MHz. To minimise the noise in the signal, a digital filter was applied, with frequency bandwidth: High-pass filter 50 kHz and Low-pass filter of 500 kHz (controllable remotely). To detect AE hits, we applied two hit detectors with fixed values, and one hit detector with a floating value that changed with the noise level, so it was set as a percentage of the noise level at the current moment. The global measurement period for AE parameters was set to 1 second, because the test was anticipated to run for a long time. The AE software was set up to record the full signal every half an hour of the test. We reached this compromise after many attempts, because recording the full signal for longer times or more frequently would mean a huge amount of data that cannot be included in the available hard discs, and it is difficult to analyse. On the other hand, it is essential to record and analyse as much data as possible.

Because the focus will be on the analysis of frequency domain of AE signal, we chose to use only one AE parameter, RMS_{AE}, which is the most commonly used time-domain parameter of AE, and it is defined as:

$$RMS_{AE} = \sqrt{\frac{1}{\Delta T}\int_0^{\Delta t} V^2(t)dt} = \sqrt{\sum_{i=1}^{N}\frac{V^2(i)}{N}} \quad (1)$$

Where ΔT is the integration time constant, N is the number of discrete AE data points within ΔT, and $V(i)$ is the voltage values of the signal from the sensor.

The AE signal analysis

Two methods were considered for analysing the AE signal. These were the Short-time Fourier Transform (STFT), and Welch method. Both methods depend on the Fast Fourier Transform (FFT), which is a classic spectrum analysis method used to analyse nonstationary signals (such as AE) to transform the AE signal waveform into its frequency spectrum.

STFT is a sequence of Fourier transforms that are applied to sliced (windowed) signal, and it is used to analyse the changes of the frequency content of a nonstationary signal over time, because it provides the time-localised frequency information for situations in which the frequency components of a signal vary over time. While the standard Fourier transform provides the frequency information over the entire signal time [35]. STFT was proposed by D. Gabor [36], where the signal (especially if it is considered as a nonstationary signal) is divided into smaller segments, and then the Fourier transform is calculated for each segment. The length of each segment is the same, it is L. For a continuous-time signal x(t), the STFT coefficients can be represented mathematically using the following:

$$X(\tau,\omega) = \int_{-\infty}^{\infty} x(t).w.(t-\tau).e^{-j\omega t}.dt \quad (2)$$

Where $X(\tau,\omega)$ is the Fourier transform, π and ω represent the time and frequency axes, respectively, and w is the window function.

The STFT spectrogram is a 3D graph that represents time, frequency, and magnitude values. It is typically colour-coded for the magnitude range, where a lighter colour represents a higher magnitude value, as can be seen in Figure 5.

It is obvious that STFT is more accurate than the standard FT, especially for nonstationary signals, because it has smaller time frames; consequently, the frequency spectrum moves more smoothly over time.

On the other hand, we can apply Welch method, which is a method based on time averaging over short modified periodograms that uses FFT for estimating power spectral densities (PSDs). The principle of this method is to divide the time signal into successive overlapping blocks (windows), forming the periodogram for each block, and then averaging [37]. So if we have:

$$x_m(n) = x.(n + m.N)$$

Where n = 0, 1, . . . , N-1 refers to the mth block of signal x, then the Welch estimate is given by:

$$\hat{R}_x(\omega k) = \frac{1}{M}\sum_{m=0}^{M-1}\left|DFT_k(x_m)\right|^2 \triangleq \left\{\left|X_m(\omega k)^2\right|\right\}_m \quad (3)$$

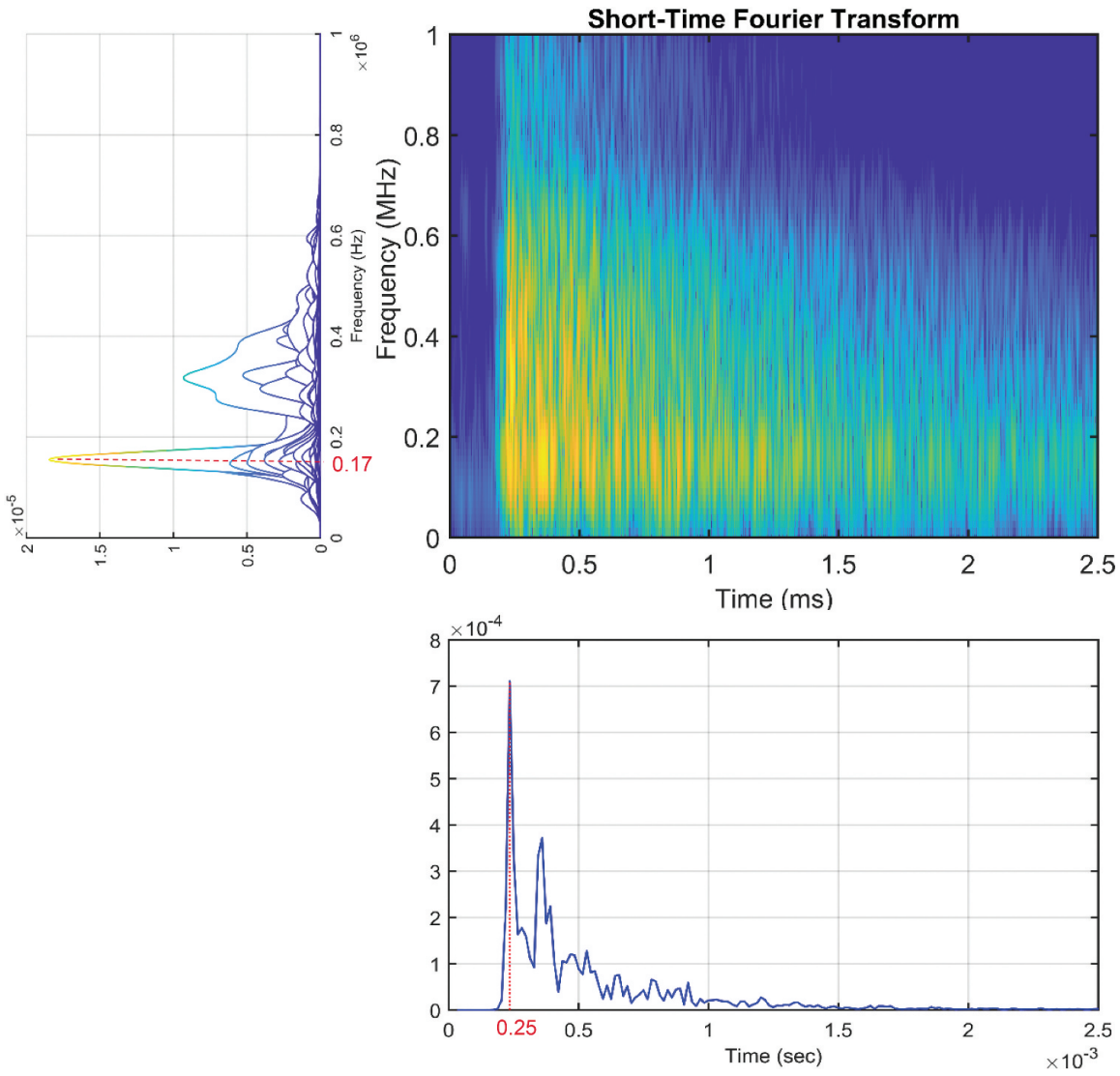

Figure 5. The STFT spectrogram of an AE, with its time and frequency components below and to the left, respectively.

Where '$\{.\}_m$' indicates the time averaging across blocks of data indexed by m.

However, in this work, we used the functions available in MATLAB© to calculate the STFT spectrogram and Welch PSD for the AE signal.

So basically, the main difference between Welch and STFT is that in the first, we average all the results of the windows, and in the second, we place them side by side as a coloured 3D graph, where the intensity of the colour represents the third dimension. The end goal is to determine the dominant frequency of AE hits. The DF is defined as the frequency corresponding to the highest point of amplitude in the two-dimensional (2D) spectrum, and it is more complicated and time consuming to obtain peaks from the 3D spectrogram than from the Welch PSD estimate.

Therefore, because of its effectiveness, significant saving in computation time, and for its accuracy, Welch method has been chosen to be used for the rest of the analysis to get the DFs of AE hits.

To extract AE hits from the recorded AE signal, we define a post-processing hit detector (PPHD) with a specific detection threshold and then we run the MATLAB code on the recorded data again. The parameters of the PPHD that we specified for the presented results are given in Table 2:

In this table, the detection threshold was chosen according to values from previous tests, so it was set to be exactly above the noise level, but not high to lose valid signal. Separation time is the time during which the signal must remain below the threshold to activate the detector for a new hit detection. Dead time is when the signal remains below the threshold to consider the current hit ended. Minimum and Maximum hit lengths are the limits for the AE hit to be considered valid. The window size represents the number of samples in a duration, and it was chosen from a list of fixed values provided by the software, while the window overlap was chosen to be 50% as a tradeoff between computation time and resolution.

It is worth mentioning that changing the values of the PPHD parameters such as 'window size' and 'overlap' would influence the time required for the analysis and the smoothness of the PSD curves, while PPHD parameters such as 'separation time', 'dead time', 'minimum and maximum hit lengths' have an effect only on the number of valid hits but not on the trends in the graph. However, changing the detection threshold value of PPHD usually causes big change in the results, and it should be chosen carefully from the beginning, because it is related to the strength of the signal. This threshold could be changed for different phases of the test, but for the purpose of comparison we chose to keep one threshold detection value for the whole test, which was set slightly above the AE signal strength in the period of smooth running of the bearing after the running-in period until the beginning of pitting.

The resulting AE hits from the PPHD are normal AE hits, as shown in Figure 6 where we can see that the hit detector (horizontal green line) is set at 0.5 mV. Some of the hit parameters are shown below the figure.

After extracting a complete list of AE hits detected by the PPHD, we apply the FFT on each hit to transform from the time domain to the frequency domain using Welch method. The result of each transform is the PSD estimate, as shown in Figure 7.

The sequence used in this study for signal processing of AE was as follows: the AE signal was received from sensor A (it is connected to the card A in the AE analyser, whereas sensor B is connected to the housing, as shown in Figure 4). The signal was fully recorded with a sampling frequency 5 MHz for 10 seconds every half hour of the test. Then, a hit detector called the post-processing hit

Table 2. Parameters of the PPHD.

Parameter	Value
Detection threshold	0.5 mV (54 dBAE)
Separation time	1 ms
Dead time	10 ms
Minimum hit length	1 ms
Maximum hit length	500 ms
FFT Calculation method	Welch estimate
Window type	Welch window
Window size	8192
Window overlap	50%

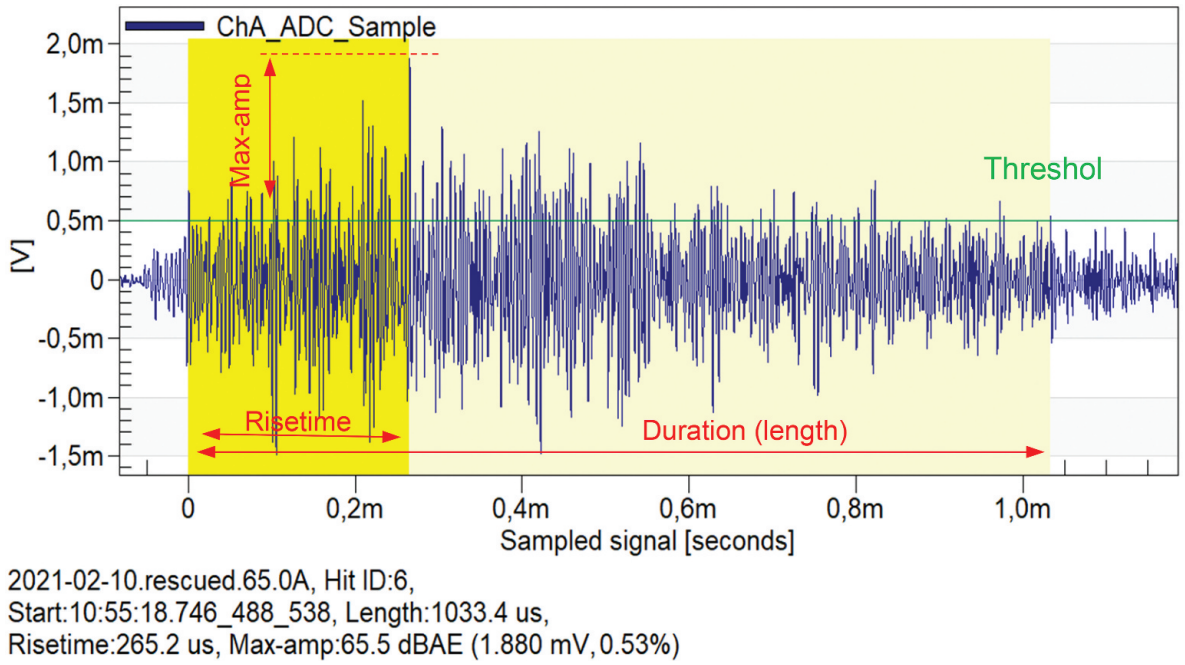

Figure 6. A sample AE hit detected by the PPHD.

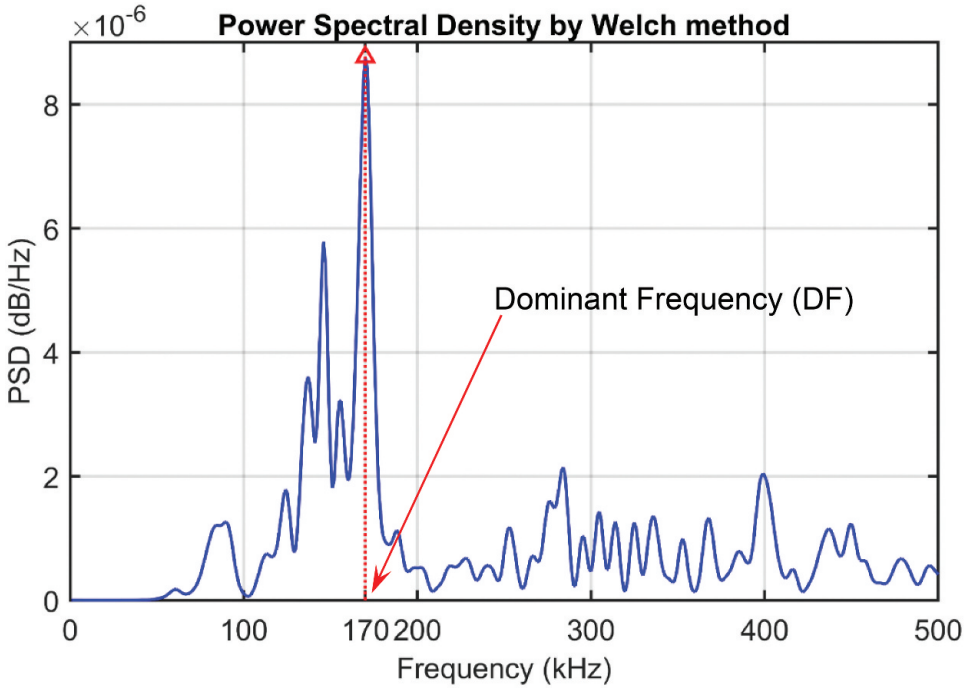

Figure 7. Power spectral density of the AE hit shown in Figure 6 above.

detector PPHD was created, which was then applied to the recorded signal for the entire test (offline, after the end of the actual test). We took each detected hit and applied the Fast Fourier Transform (FFT) on it to transform the signal from the time domain to the frequency domain. As mentioned previously, for this work we adopted the Welch method. Then we identified the dominant frequency (DF) of each hit.

These steps are shown in Figure 8 as they were applied in the analysis process.

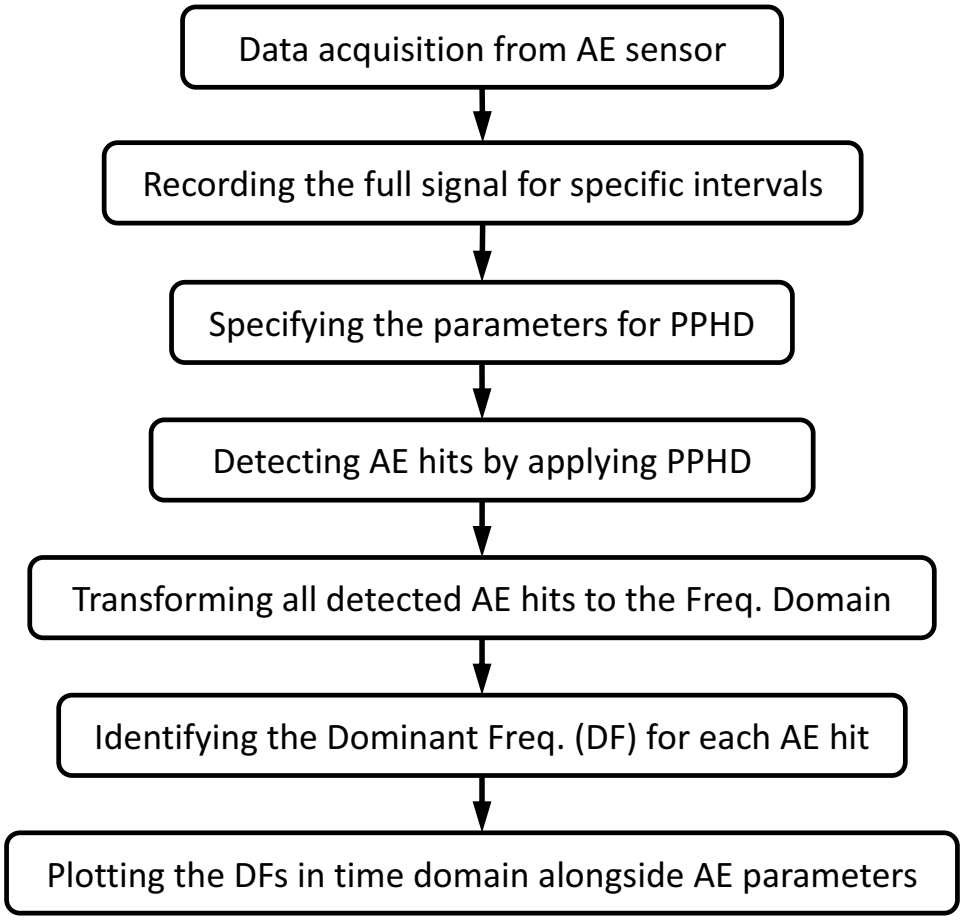

Figure 8. Sequence of steps for AE signal analysis.

It is worth mentioning here that the application of AE was carried out according to the standard ISO 22,096:2007 [38].

Results

One sample of the results of this analysis is shown in Figure 9, where Figure 9(a) shows the temperature and vibration levels on the outer ring of the tested bearing, and Figure 9(b) shows the RMS_{AE} value and the DFs of AE hits that are detected by PPHD; therefore, this figure was called the DF map of the entire test. The green curve represents the incremental increase in the sum of AE hits during the full test. Since the majority of events for this measurement occur during the first 10 hours and the last 12 hours, we present Figures 11 and 13, which are essentially parts of Figure 9 with concentration on those two periods.

From Figure 9(a), we can see that the vibration signal (black line), which represents the raw acceleration value received from the vibration transducer, reflected the changes in the condition of the bearing during the last period of the test, but it did not capture the changes in the first period (the running-in period). While the temperature of the outer ring was not responsive enough, and the range of change in temperature (around 20 C°) was small and could not be depended upon. On the other hand, Figure 9(b) gives an obviously more detailed picture of the same measurement using AE. The red line that

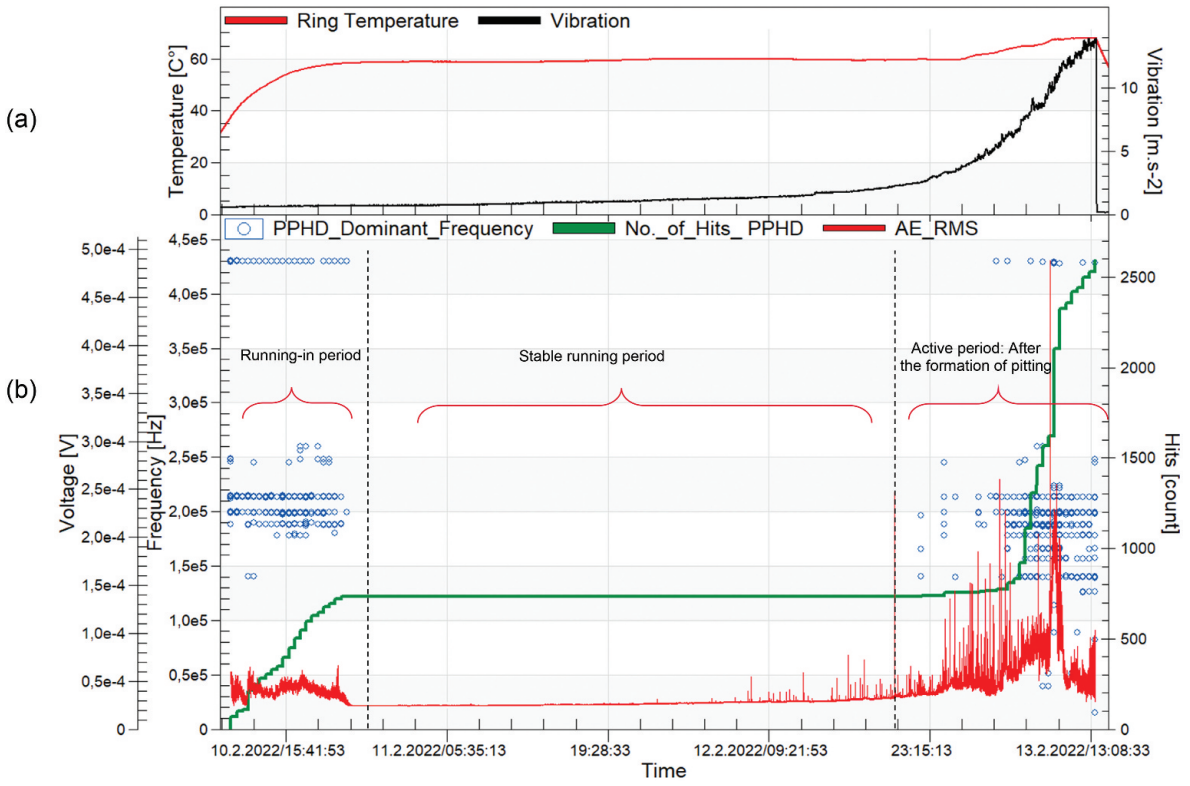

Figure 9. Temperature, vibration, RMS_{AE}, and DFs of AE hits for the whole period of the measurement (DF map of the entire test).

represents the RMS_{AE} (measured in volts on the left axis) shows at the first couple of hours the running-in period, which is the initial process that occurs when solid surfaces are brought together under a non-zero normal force. It clearly shows an increase in AE activity because of the breaking of the tips and abnormalities left on the surface of the bearing raceways and rollers as a result of machining. The removal of these abnormalities because of the large pressure between the rollers and the raceways in the loading zone makes the raceways surface smoother as shown in Figure 10, which shows photos of the bearing rings taken after the end of the running-in period in one of the five tests that was carried out.

The RMS_{AE} curve in Figure 9, then shows the stable running period which continues for a couple of days. This is the useful service period of the bearing, and it is preferred to be as long as possible while the bearing is in service, but in our experiments, this period is not useful since it is inactive, as the graph of RMS_{AE} shows. Figure 9 shows the DFs of AE hits as small blue circles, and we can see that they disappear almost completely during the stable running period. This is partly because of the parameters that were chosen for the PPHD, which are given in Table 2, and partly because of the filtration parameters in the AE analyser. In fact, the existence of DFs of AE hits during the running-in period gives more credibility to the results because the parameters were applied uniformly throughout the experiment. These DF values during the running-in period show that all DFs of AE hits fall in eight discrete and well-defined bands. Since this period continues for a few hours and then disappears, it is not important per se, but it is a proof of the effectiveness of using AE over vibration, since

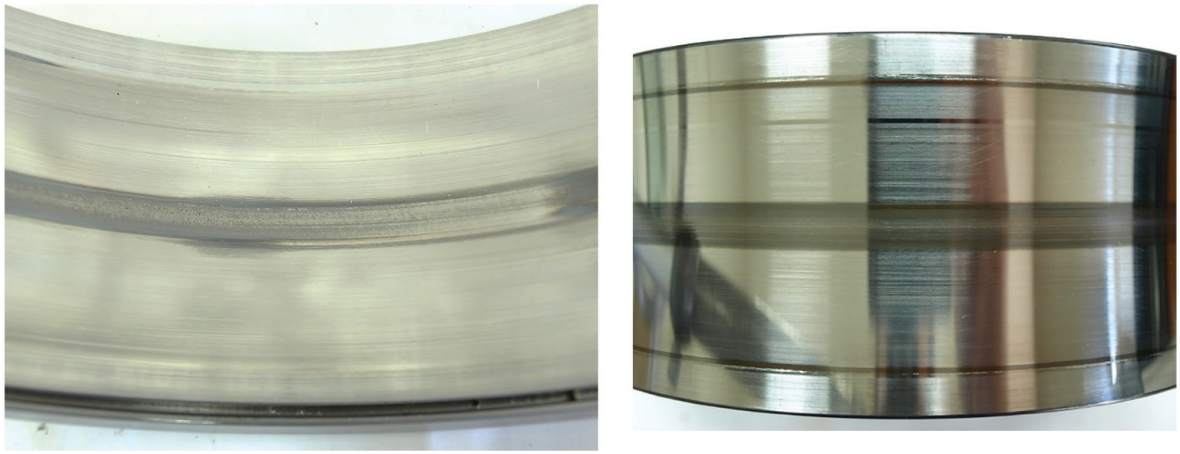

Figure 10. The smoothness of the raceways of the outer and inner rings after the running-in period.

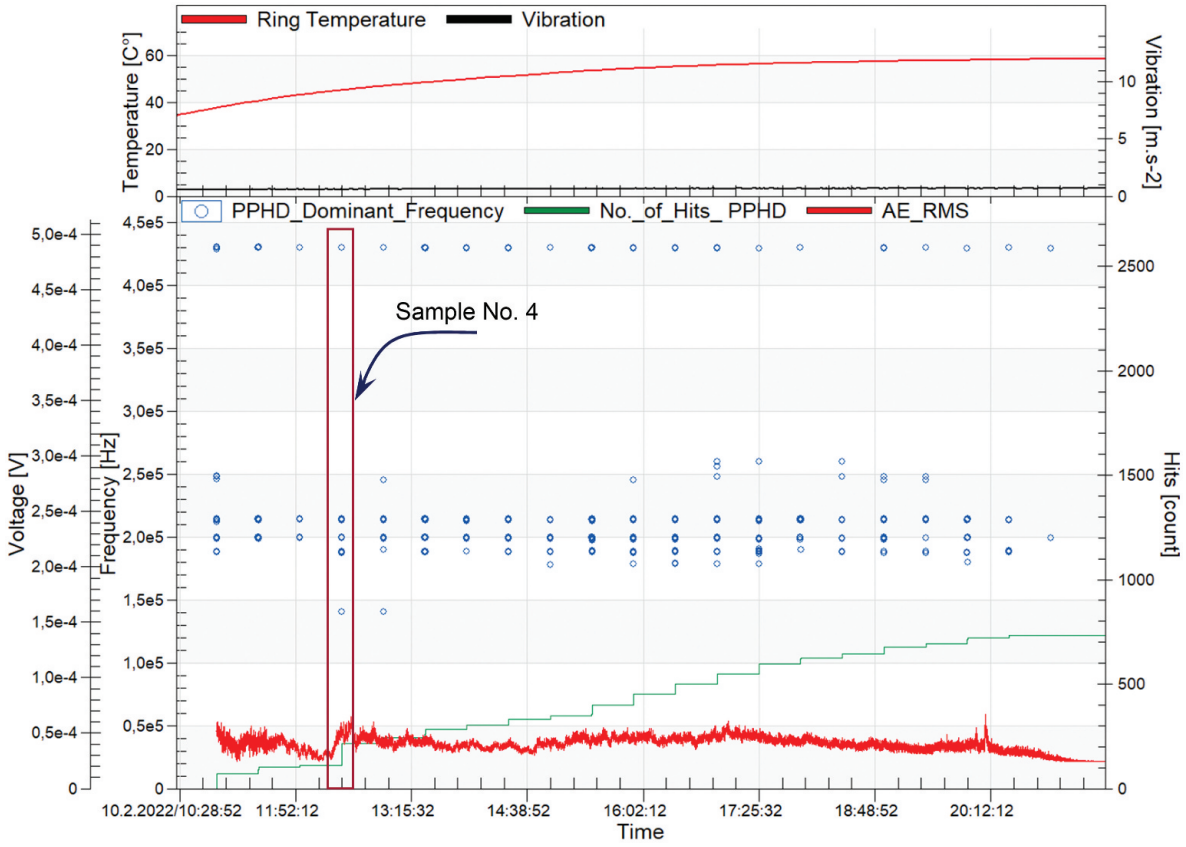

Figure 11. Temperature, vibration, RMS_{AE} and AE DFs for the period of first 10 hours (the running-in period).

vibration curve did not clearly reflect the existence of it in its curve. The analysis of the signal in this period is also important for comparison purposes, as we know for sure that this is the running-in period, hence we know the origin of AE hits is in this period.

Figure 11 shows a concentration 'magnification' on the first 10 hours of the whole test where the running-in takes place.

The figure shows 21 columns of blue circles, where each column represents 10 seconds out of 30 minutes of the fully recorded signal (i.e. about 10 hours). These columns are the places where the signal was fully recorded and then analysed by producing a list of DFs of all PPHD hits. Each column continues for just 10 seconds out of 30 minutes because recording the full signal continuously with the specified testing parameters and sampling frequency is impractical and it does not provide extra information.

Sample number 4 from these 21 columns was further analysed because it contained the highest increased number of hits detected by PPHD, represented by their DFs.

The 'magnification' of column number 4 from Figure 11 is shown in Figure 12. The time slice for this sample lasted from 10 February 2022/12:25:18 to 10 February 2022/12:25:28.

From this figure, we can clearly see 8 frequency bands that are separated and distributed to ranges shown in Table 3. This specific distribution of DFs of AE hits was repeated in all other time slices (columns of blue circles in the figure). The sum of all DFs of AE hits in the running-in period was then summarised and analysed statistically.

After the running-in period, comes a long stable running period, where PPHD did not capture any hits. As stated before, this period corresponds to the useful life of the bearing, and the set-up of PPHD was calibrated intentionally to make the number of hits in this period as low as possible. However, once defects (pitting) started to form on the raceways of the bearing, this period is considered as finished, and the PPHD started getting AE hits. Hence started the so-called active period, which is the period that starts with the beginning of first signs of pitting and continues until the end of the experiment when the vibration level exceeds a specific safety threshold. This active period in this particular experiment continued for almost 11 hours, therefore we concentrated on analysing the signal during this period, as shown in Figure 13, which is a magnification of the active

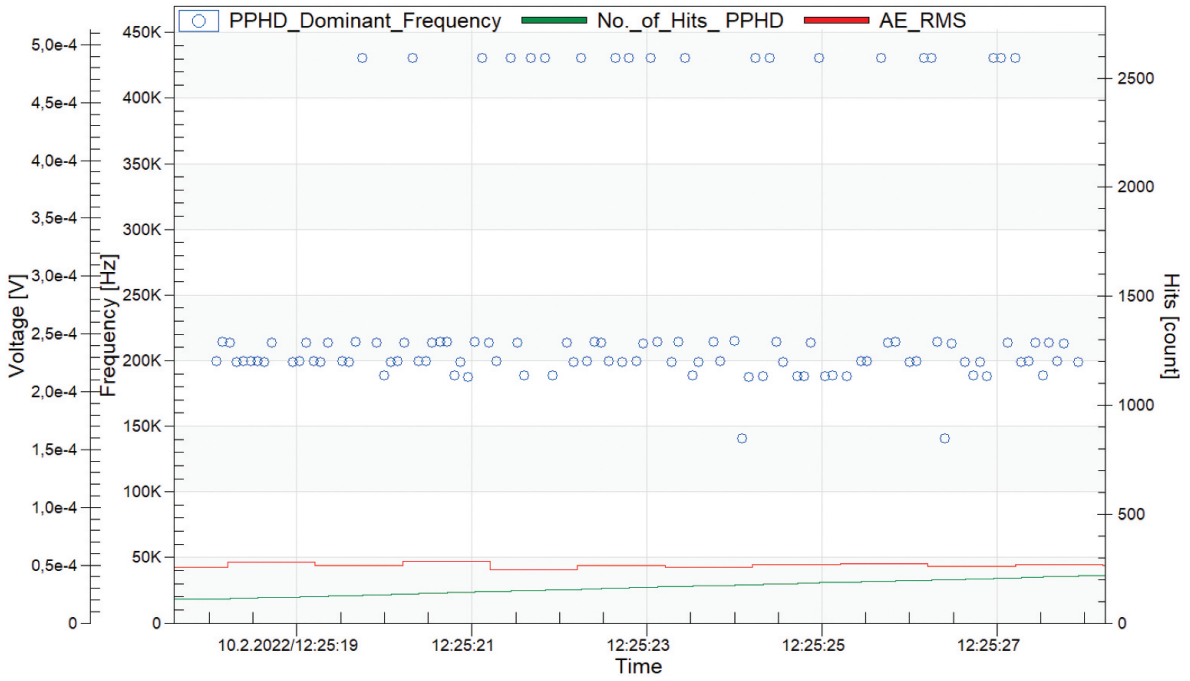

Figure 12. RMS_{AE} and AE DFs for one time slice (4^{th}) with the highest increase of AE hits in the running-in period.

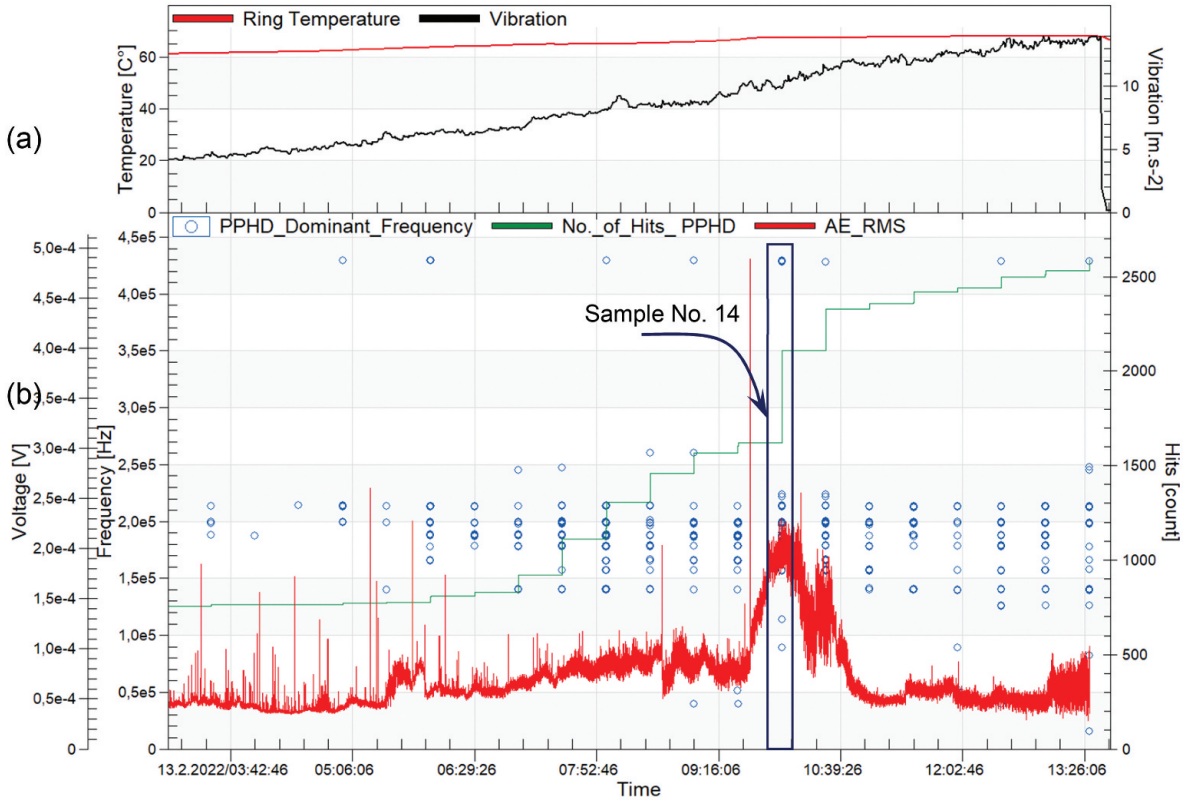

Figure 13. Temperature, vibration, RMS_{AE} and AE DFs for the active period (the last 11 hours of the measurement).

Table 3. The distribution of AE hits in the specified DF bands.

	DF bands in the running-in period (first 10 h.) (kHz)		DF bands in the active period (last 12 h.) (kHz)		
	Range (kHz)	Number of hits	Range (kHz)	Number of hits	Sum
1	429 – 431	104	427 – 429	21	125
2	260 – 263	3	260 – 261	5	8
3	245 - 248	17	245 – 248	5	22
4	222 – 225	0	222 – 225	5	5
5	212 – 216	318	213 – 216	144	462
6	197 – 201	182	196 - 200.5	495	677
7	186 – 190	98	186 – 190	275	373
8	177 – 180	8	177 – 179	424	432
9	165 – 166	0	165 – 166	243	243
10	156 – 157	0	155 – 158	52	52
11	139 – 140	4	190 – 141	168	172
12	125 – 127	0	125 – 127	5	5
13	80 – 83	0	80 – 83	6	6
14	30 – 40	0	30 – 40	12	12
		734		1860	2594

Total sum = 2594 AE hit.

period from Figure 9. In (a) part it shows the same as before that vibration increased steadily until a specific threshold that is preset to stop the test when it is reached, while the temperature's increase was insignificant. In Figure 13 (b) we see the 22 columns of blue circles that represent the DFs of AE hits.

From these columns, the sample number 14 was chosen for further analysis because, as the curve of the number of PPHD hits shows, this sample has the highest number of

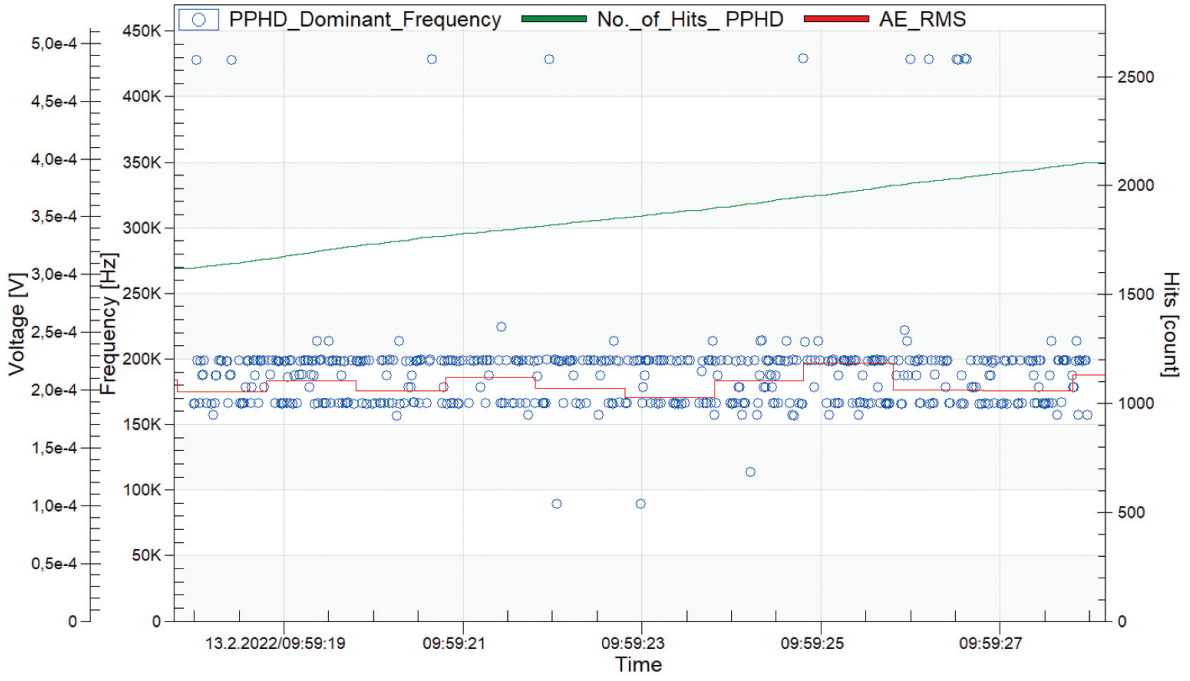

Figure 14. RMS_{AE} and AE DFs for one time slice (14^{th}) with the highest increase of AE hits in the active period.

hits. The time slice for this sample lasted from 13 February 2022/09:59:17 to 13 February 2022/09:59:27.

So 'magnifying' this time slice further gives Figure 14. This figure clearly shows the separate DF bands of AE hits. The frequency ranges of the bands are listed in Table 3.

Table 3 also includes the number of AE hits that fall within each range (frequency band).

The following graph in Figure 15 represents the results in Table 3. In this graph, the DFs of AE hits are shown to belong to 14 bands (frequency ranges). These bands were divided into high-frequency H-bands (above 220 kHz), intermediate-frequency I-bands (above 150 kHz and below 220 kHz), and low-frequency L-bands (below 150 kHz).

From the statistical representation of this specimen's results, shown in Figure 15, we can see that the number of AE hits that appear during the formation of defects (pitting and/or scaling) is higher (almost dominant) in the lower DF bands, whereas the number of AE hits that appear during the running-in period is higher in the high DF bands. This pattern was repeated when we repeat the statistical analysis of the PPHD AE hits for other time slices, and it could be seen even in a visual comparison as the one presented in Figure 16, which is the same as Figure 9 after removing the stable running period from the middle, and where the DF bands were specified by yellow lines.

Visual inspection of the tested bearing parts showed no pitting on the rolling elements, a few pits on the inner ring (the rotating ring), and a large amount of pitting and even scaling in the outer ring (the fixed ring), specifically in the loading zone. The following figures, Figures 17, 18 , and 19 show the rolling elements, inner ring, and outer ring of the tested bearing, respectively.

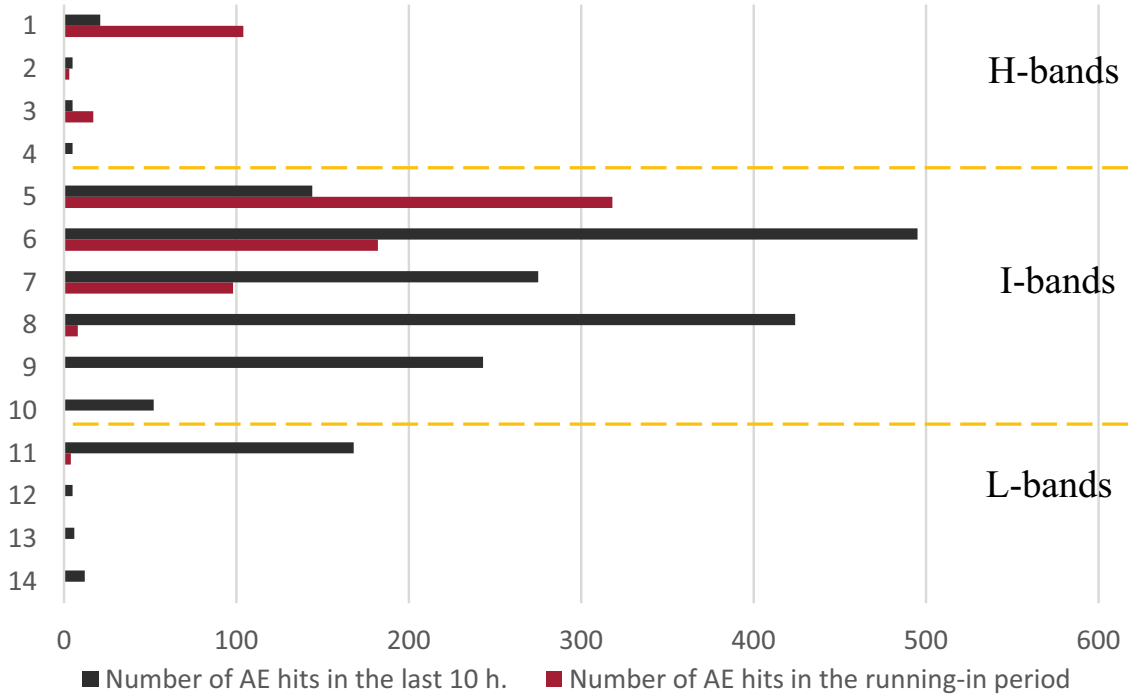

Figure 15. Comparison between the number of AE hits in the two periods where AE hits took place.

Discussion

In this study, we introduced a new method for evaluating bearing condition based on the use of the DF of AE hits as the main parameter. Along with AE as a tool for detecting damage, vibration and temperature were used for the purpose of comparison. The vibration measurements provided a realistic indication of the condition of the tested bearings, in which there was a constant increase in the vibration level with the increased number of defects on the raceways of the outer ring. On the other hand, the temperature of the outer ring did not give a good nor responsive indication for the beginning of defect formation. The temperature measurement could not indicate the end of the running-in period, as can be seen in Figure 9, even the range of change in the temperature during the last period of the test was not big enough to indicate or to follow the increased level of defects in the bearing condition.

The AE signal analysis led to the creation of the DF map, which is a representation of the DFs of all AE hits that were detected by PPHD when they were laid out alongside the RMSAE in one graph for the entire test. The analysis focused on the time slices where the signal was fully recorded, and the entire number of AE hits was processed and presented. DF maps were created for each of these recorded time slices, and a clear pattern was noticed when studying and representing them statistically. In our analysis of AE signal we used Welched method as an FFT-based transformation to the frequency domain, which turned out to be more beneficial for our purposes in this work than the STFT method as used in [26], or the wavelet packet transformation in [17].

Plotting the time domain parameter of AE (RMS_{AE}) in the DF map helped identifying the different periods of the test, since it is proven that there is a correlation between AE

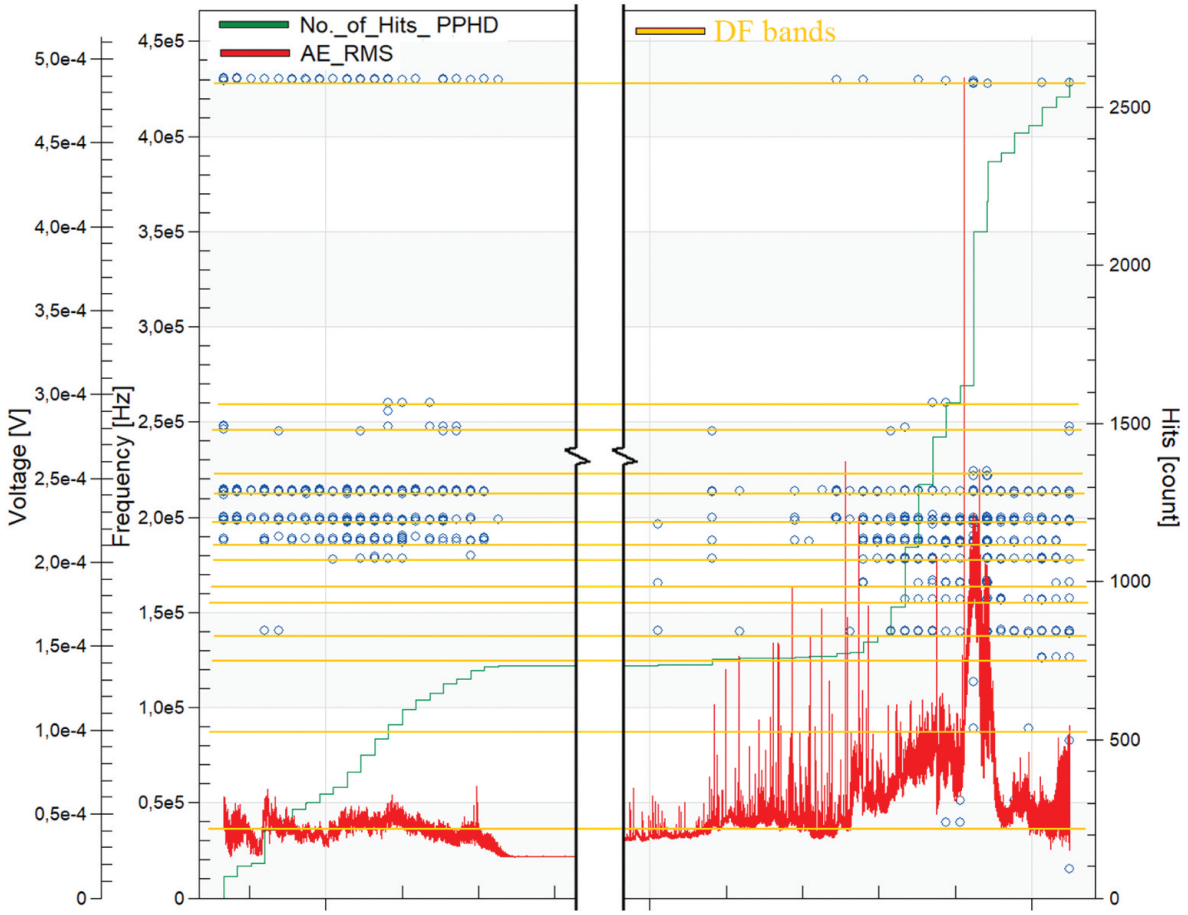

Figure 16. A comparison between the discrete AE DFs bands (the yellow lines) in the two periods at the beginning and at the end of the test.

Figure 17. Number of the rolling elements of the toroidal bearing after the test.

parameters' levels and the natural propagation and formation of bearing defects shown by the works of Van Hecke et al. [39], Elforjani and Mba [40–42] and others.

As Hase, et al. [43] showed in their correlation map of AE frequency spectra involving deformation and fracture in Figure 9, which is supported by other references [44–46],

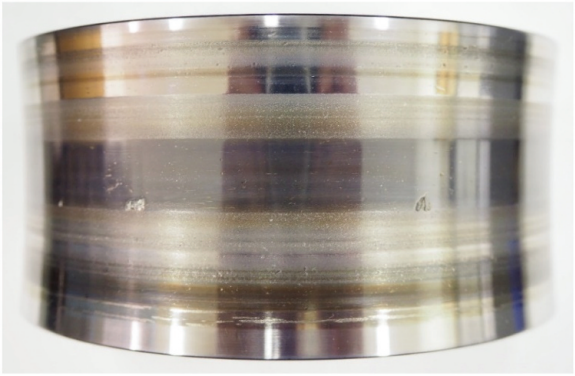

Figure 18. The scattered pitting on the inner ring of the toroidal bearing after the test.

Figure 19. The spalling in the loading zone on the outer ring of the toroidal bearing after the test (with permission from jakub.Nemecek@zkl.cz).

that the abrasive wear results in lower levels of AE frequency, whereas the adhesive wear (severe wear) results in higher levels of AE frequencies. Similarly, in this study, we showed that the events during the running-in period result in higher and more concentrated values of the DF bands than those during the defect formation period, i.e. the last phase of the tests. The results of this study were more precise in defining the values at which the DF bands of each period are more dominant, as shown in Table 3 and the corresponding Figure 15. Therefore, choosing DF of AE hits as the main parameter to monitor the condition of the tested bearing was proven to be the right choice. Supportive evidence could be found in conclusions of other researchers, such as XU et al. [15] where they stated clearly that the peak frequency of AE signal is the best feature selected to identify the damage modes, due to the high discrete degree of AE signals in fibre joints. We used similar procedures to extract this peak frequency, we just followed the norm of calling it the dominant frequency (DF), since those two terms are used interchangeably as shown by a study of the Time-Frequency domain characteristics of AE signal [47], and as in many other works used this term, such as [21,22,24,25].

As mentioned earlier, the curve of RMS_{AE} was plotted as part of the DF map to help identify the different periods of the test, because the correlation between AE time-domain parameters and the formation of bearing defects is well-established, while the use of DF of AE hits is still new and cannot be used independently.

Vibration measurement was also used as a solid reference because it is a well-established method. This limitation of the new method can be solved over time by doing more measurements and building bigger databases that relate each type of defect to a specific DF.

Another limitation is that, for logistical reasons, we could not record the whole AE signal for the whole test, since this would require storage for huge amount of data, and would make it difficult to process this data. But since recording the whole AE signal is essential for the PPHD, we recorded 10 seconds every half hour of the test, which is a reasonable tradeoff that we reached according to experience. The creation of PPHD helped in mitigating another limitation, which is the sensitivity to noise in the signal, because in PPHD analysis we were able to change the parameters of detection even after the end of the test to guarantee cleaner data.

The use of AE time-domain parameters, as proven by many research works [39,41,43,45], can detect the initiation of defect development in the bearing's raceways, but we argue that it is not enough to give a full picture of the damage process. Furthermore, the increase in the intensity or value of these time domain parameters is correlated to the increase in the defect development process in bearings or in similar assets, but those correlations and this correspondence are not quantified. Which means it cannot be automated or integrated in an automated preventive maintenance process. While the proposed method of using the number of DFs of AE hits generate numbers, which is a significant benefit because the resulting numbers can be dealt with easily by snippet of codes in MATLAB® or in other programming languages when an automation process is considered.

Conclusion

In this work, experiments were carried out on five specimens of newly produced TRBs in a specially designed testing rig using AE as the main CM technique of the bearing, and vibration as a reference signal. Temperature of the outer ring was also measured, but this parameter was considered unreliable because the range of change was small, and the response time was long. Axial and angular displacements of the TRBs were restricted in the test rig, to minimise the number of variables. Time domain parameters of AE were extracted, but the focus was on the frequency domain parameters, specifically on the DF of AE signal. FFT and FFT-based methods were considered for transforming to the frequency domain, and Welch method was utilised for reasons related to the accuracy of obtaining the exact value of DF and the computation time with high sampling frequency. A PPHD was established to give the ability to analyse the signal after the end of the experiment and to mitigate the limitation of predetermined parameters for the whole test. PPHD requires recording the whole AE signal, but this was tackled by recording evenly-distributed time segments.

The resulting DFs of AE hits were naturally distributed to different discrete frequency ranges. These ranges were plotted in one graph for the entire test and were grouped into three major bands. This layout of DFs of AE hits on the time domain combined with one of the AE parameters (RMS_{AE}) was called the DF map.

The frequency bands in the DF map were statistically studied, and the results showed that during the running-in period the number of AE hits with DFs in the

H-band (above 220 kHz) was significantly larger than the number of DFs during the defects formation period, and they were concentrated in the highest band (approximately 430 kHz). In the intermediate frequency bands, the number of DFs was obviously larger than in other bands, and this number is a combination of AE hits from both periods, the running-in and the active last 12 hours. However, it is noticeable that the number of DFs in the running-in period always occupies the upper portion of this band. It should also be considered that this band is the most contaminated with DFs of invalid hits that are results of unfiltered noise, a limitation that cannot be avoided even with the flexibility provided by PPHD. The number of AE hits with DFs in the L-bands was relatively low, and it was composed entirely of hits from the active period of defects formation in the last 12 hours. The practical usefulness of these results increased by integrating the knowledge of the defects' nature and their sources in each period, as shown in the literature, so that we can correlate the nature of those sources with the number of AE hits and their DFs. This provides a great opportunity to not only predict the period of defects formation but also to quantify the deterioration of the bearing. This key aspect of the quantification of the bearing condition gives the ability to build more accurate and automatable preventative CM systems, which is an essential part of the next step we are planning when implementing those results on different types of roller bearings.

Acknowledgments

This research was supported by the National Competence Centre of Mechatronics and Smart Technologies for Mechanical Engineering under the project TN02000010, and it is co-financed by the Technology Agency of the Czech Republic (TACR), within the National Centre of Competence Program. The authors would also like to thank ZKL R&D Center for their cooperation.

Disclosure statement

No potential conflict of interest was reported by the author(s).

Funding

This work was supported by the Technology Agency of the Czech Republic [TN02000010].

ORCID

Housam Mohammad http://orcid.org/0000-0003-2955-7112
Frantisek Vlasic http://orcid.org/0000-0002-5283-2461
Baraah Maya http://orcid.org/0000-0002-9868-2358
Mhd.Ali Shehadeh http://orcid.org/0000-0001-5550-4650
Pavel Mazal http://orcid.org/0000-0003-1766-4666